2013-06-12

Facile Synthesis of Pd-Ir Bimetallic Octapods and Nanocages Through Galvanic Replacement and Co-Reduction, and their use for Hydrazine Decomposition

UTD AUTHOR(S): Ning Lu, Jinquo Wang and Moon J. Kim

PCCP

RSC Publishing

PAPER

View Article Online
View Journal | View Issue

Cite this: *Phys. Chem. Chem. Phys.*, 2013, **15**, 11822

Facile synthesis of Pd–Ir bimetallic octapods and nanocages through galvanic replacement and co-reduction, and their use for hydrazine decomposition†

Maochang Liu,[ab] Yiqun Zheng,[c] Shuifen Xie,[a] Naixu Li,[a] Ning Lu,[d] Jinguo Wang,[d] Moon J. Kim,[d] Liejin Guo[b] and Younan Xia*[ac]

Received 8th May 2013,
Accepted 20th May 2013

DOI: 10.1039/c3cp51950c

www.rsc.org/pccp

This article describes a facile synthesis of Pd–Ir bimetallic nanostructures in the forms of core–shell octapods and alloyed nanocages. The success of this synthesis relies on the use of Pd nanocubes as the sacrificial templates and interplay of two different processes: the galvanic replacement between an Ir precursor and the Pd nanocubes and the co-reduction of Pd^{2+} and Ir^{3+} by ethylene glycol. The galvanic replacement played a dominant role in the initial stage, through which Pd atoms were dissolved from the side faces whereas Ir atoms were deposited at the corner sites to generate Pd–Ir core–shell octapods. As the concentration of Pd^{2+} in the reaction mixture was increased, co-reduction of Pd^{2+} and Ir^{3+} occurred in the late stage of synthesis. The resultant Pd and Ir atoms were deposited onto the octapods while the Pd atoms in the interiors continued to be etched away due to the galvanic replacement, finally leading to the formation of Pd–Ir alloyed nanocages. The octapods and nanocages were then evaluated as catalysts for the selective generation of hydrogen from the decomposition of hydrous hydrazine. The nanocages exhibited better selectivity for hydrogen generation than octapods (66% *versus* 29%), which can be attributed to the presence of an alloyed, porous structure on the surface.

Introduction

Hydrogen is widely accepted as a future source of clean energy that can address issues related to environmental pollution, climate change, and expensive oil prices.[1–9] Many types of nanomaterials have been explored as catalysts for the generation of hydrogen from a rich variety of chemical compounds or materials. Owing to its high hydrogen content (8.0 wt%), hydrazine is considered as one of the most promising chemical compounds for hydrogen storage.[10–15] Historically, it has also been employed as a propellant to provide power sources for unmanned space vehicles and submarines.[12] However, it remains a critical challenge to develop a catalyst with high activity and H_2 selectivity (see ESI† for a definition of H_2 selectivity) at room temperature for the decomposition of hydrazine.

Iridium nanoparticles have been widely used to catalyze the decomposition of hydrazine. However, they only exhibited high H_2 selectivity when the decomposition was conducted at high temperatures (typically, >300 °C).[16–18] In general, binary noble-metal nanostructures are of interest for a wide variety of applications, including decomposition of hydrazine, owing to their tunable elemental compositions.[19,20] Recently, Xu and coworkers reported a catalyst based on bimetallic nanoparticles for the decomposition of hydrazine.[21–24] They were able to achieve a 100% H_2 selectivity at room temperature when Ni–Ir alloyed nanoparticles were used as the catalyst.[23] Such an improvement not only significantly reduced the material cost of a catalyst, but also provided an alternative route for promoting the catalytic performance by focusing on Ir-based bimetallic nanoparticles.

Despite this and other successful demonstrations, it is worth pointing out that the bimetallic nanoparticles that have been

[a] *The Wallace H. Coulter Department of Biomedical Engineering, Georgia Institute of Technology and Emory University, Atlanta, Georgia 30332, USA. E-mail: younan.xia@bme.gatech.edu*
[b] *International Research Center for Renewable Energy, State Key Laboratory of Multiphase Flow, Xi'an Jiaotong University, Xi'an, Shaanxi 710049, P. R. China*
[c] *School of Chemistry and Biochemistry, School of Chemical and Biomolecular Engineering, Georgia Institute of Technology, Atlanta, Georgia 30332, USA*
[d] *Department of Materials Science, University of Texas at Dallas, Richardson, Texas 75080, USA*

† Electronic Supplementary Information (ESI) available: TEM and XPS data of Pd–Ir bimetallic nanostructures obtained at different stages of a standard synthesis; TEM images of Pd–Ir nanostructures obtained using the standard procedure except for the use of different reaction temperatures; TEM images of Pd nanostructures after going through the standard procedure in the absence of an Ir precursor. See DOI: 10.1039/c3cp51950c

evaluated were obtained without a precise control over morphology and size distribution. They were often polycrystalline aggregates with random, unknown facets exposed, according to the electron microscopy images reported. As a result, it could be risky to attribute the enhancement in catalytic performance to a single parameter such as the variation in elemental composition. It is also challenging to make the same catalyst from batch to batch and achieve a good understanding of the effects of size and morphology. The arguments would be more convincing if those catalysts were fabricated with a well-defined structure and narrow size distribution. In fact, the surface structure has been demonstrated with a strong impact on the catalytic performance.[25–31] For example, Pt nanoparticles with an unusual tetrahexahedral shape were found to exhibit enhanced (up to 400%) catalytic activity for formic acid oxidation reaction (FOR) and ethanol oxidation reaction (EOR) when compared with the conventional particles.[31] Recently, bimetallic nanostructures with concave structures or hollow interiors (cages, boxes, frames) were also found to affect the performance of a catalyst. This is because such a surface contained high densities of atomic steps and kinks and thus provided more active sites for the catalytic reaction to occur.[32] This principle could be possibly employed to enhance the catalytic performance of bimetallic nanostructures by maneuvering their morphologies to include either concave surfaces or hollow interiors.

Herein, with Pd nanocubes as sacrificial templates, we have developed a facile synthesis of Pd–Ir bimetallic nanostructures in the forms of core–shell octapods and alloyed nanocages. Thanks to the use of Pd nanocubes in high purity and good uniformity, both types of bimetallic nanostructures could be obtained with a well-defined morphology and narrow size distribution. The key to the success of morphology control relies on the interplay of two major processes: galvanic replacement between Pd nanocubes and an Ir precursor and the co-reduction of Ir^{3+} and Pd^{2+}. Both types of bimetallic nanostructures could catalyze the decomposition of hydrazine at room temperature. Thanks to the presence of an alloyed, highly porous structure on the surface, the nanocages exhibited much higher H_2 selectivity relative to the octapods (66% *versus* 29%).

Experimental section

Chemicals and materials

Sodium tetrachloropalladate(II) (Na_2PdCl_4, 99.998%), iridium(III) chloride hydrate ($IrCl_3{\cdot}xH_2O$, 99.9%), poly(vinyl pyrrolidone) (PVP, $M_w \approx 55\,000$), and ascorbic acid (AA) were obtained from Sigma-Aldrich. Potassium bromide (KBr) was obtained from Fisher Scientific. Potassium chloride (KCl) and ethylene glycol (EG) were purchased from J. T. Baker. All chemicals were used as received. The water used in all syntheses was de-ionized water with a resistivity of 18.2 MΩ cm.

Synthesis of Pd nanocubes

The Pd nanocubes were synthesized according to our previous report.[33] In a typical synthesis, 8.0 mL of an aqueous solution containing 105 mg of PVP, 60 mg of AA, and different amounts of KBr and KCl was hosted in a vial and pre-heated to 80 °C in an oil bath under magnetic stirring for 10 min. Subsequently, 3.0 mL of an aqueous solution containing 57 mg of Na_2PdCl_4 was added using a pipette. After the vial has been capped, the reaction was allowed to continue at 80 °C for 3 h. We obtained Pd nanocubes of different sizes by varying the amounts of KBr and KCl. For example, Pd nanocubes of roughly 18, 10, and 6 nm in size were obtained by the use of 600 mg of KBr, 300 mg of KBr, and a mixture of 5 mg of KBr and 185 mg of KCl, respectively. The product was collected by centrifugation, washed three times with water, and re-dispersed in 11 mL of EG for future use.

Preparation of Pd–Ir bimetallic octapods and nanocages

For a standard synthesis of Pd–Ir bimetallic nanocrystals, 1 mL of the suspension of Pd cubes (18 nm in size) and 7 mL of EG containing 33.3 mg of PVP and 300 mg of KBr were mixed in a 25 mL three-necked flask. The mixture was heated to 130 °C in air under magnetic stirring for 10 min. Meanwhile, 6 mg of $IrCl_3{\cdot}xH_2O$, was dissolved in 3 mL of EG and then added into the as-prepared mixture containing PVP, KBr, and Pd cubes using a syringe pump at an injection rate of 1.5 mL h^{-1}. The reaction was allowed to continue in air at 130 °C for 24 h. The mixture was then centrifuged and washed once with acetone and three times with deionized water. The final products were re-dispersed in 3 mL of deionized water for characterization and catalytic test.

Catalytic decomposition of hydrazine monohydrate

Catalytic reactions were carried out at room temperature using a protocol described by Xu and coworkers.[21–24] Typically, 0.4 mL of an aqueous suspension of the Pd–Ir bimetallic nanocrystals and 0.01 mL of hydrazine monohydrate were sequentially injected into a two-neck flask kept at 20 °C, with one of the openings connected to a gas burette. The gases produced were passed through a trap containing 100 mL of hydrochloric acid (1.0 M) to ensure absorption of ammonia. The volume of the remaining gas was monitored by the gas burette. The stability of the Pd–Ir bimetallic catalyst was examined by repeating the reaction several times over the same catalyst by adding an equal amount of hydrazine monohydrate to the reaction vessel after completion of the previous run. The catalyst was separated from the reaction mixture by centrifugation and washed with deionized water once for TEM characterization.

Characterization

Transmission electron microscopy (TEM) images were taken using an H-7500 microscope operated at 75 kV (Hitachi, Tokyo, Japan). High-resolution TEM (HRTEM), high-angle annular dark-field scanning TEM (HAADF-STEM), and energy dispersive X-ray (EDX) analyses were performed using an ARM200 microscope with a STEM Cs corrector and operated at 200 kV (JEOL, Tokyo, Japan). The samples were prepared by dropping aqueous suspensions of the nanoparticles onto carbon-coated copper grids (Electron Microscope Sciences, Hatfield, PA) and dried in air. The X-ray photoelectron spectroscopy (XPS) data were recorded using a

Thermo K-Alpha spectrometer with an Al Kα source (1468.6 eV) (Thermo Fisher Scientific, Waltham, MA). The samples for XPS test were prepared by drying drops of the aqueous suspension of nanoparticles on silicon substrates.

Results and discussion

As shown by Fig. 1a, the Pd cubes could be readily prepared with a uniform shape and narrow size distribution. For a standard synthesis of Pd–Ir bimetallic nanostructures, Ir precursor solution was slowly pumped into a suspension of the Pd cubes at an elevated temperature. The Pd cubes were slightly truncated at the corners (Fig. S1a, ESI†) and minor growth of Ir at the corner sites was observed at t = 1 h (Fig. S1b, ESI†). The deposition of Ir could be clearly observed after the reaction has proceeded for 2 h (Fig. 1b). At this point, the overall shape was like an octapod consisting of eight short arms with enlarged bumps at the tips. After the reaction has been continued for 9 h, a number of pores were found on the surfaces of the Pd–Ir nanocrystals (Fig. S1c, ESI†). As the reaction proceeded, the Pd and Ir atoms derived from co-reduction would still be preferentially deposited at the corner sites. However, some of the Pd and Ir atoms might also diffuse to the adjacent side faces, as shown in our recent work.[34] Eventually, the Pd cubes were transformed into Pd–Ir alloyed nanocages with hollow interiors at t = 24 h (Fig. 1c). The average sizes of the octapods and nanocages were 20 nm and 25 nm, respectively. This is because Ir atoms were deposited on the Pd cubes along the [111] directions as the reaction proceeded. Such a shape evolution process was similar to what we have observed in the case of Pd–Pt concave nanocubes and nanocages, respectively.[35,36] Two major processes – the galvanic replacement between Pd cubes and the Ir precursor and the co-reduction of Pd^{2+} and Ir^{3+} – were responsible for the sequential formation of nanostructures with the two unique morphologies.

To clarify the morphology, structure, and composition, the resultant Pd–Ir nanocrystals were further characterized by Cs-corrected HAADF-STEM, HRTEM, and EDX mapping. Fig. 2a and b, shows HAADF-STEM images of the Pd–Ir octapods and nanocages, revealing that the nanostructures maintained cubic symmetry, with a slight increase in size. For the nanocages, a lighter contrast was observed in the center relative to the edge, implying the formation of a hollow interior. Fig. 2c and d, shows HRTEM images of an octapod and a nanocage along the [100] zone axis. Further measurements indicated that the octapods were enclosed by {530} high-index facets together with a smooth surface (Fig. S2b, ESI†). In comparison, the nanocages were covered by a rough and porous surface, which could not be easily indexed. However, it was believed that there were also atomic kinks and steps on the rough surface (Fig. S2b, ESI†). Moreover, the continuously oriented lattice fringe with a uniform spacing distance implies that the nanostructures were single crystals. For face-centered cubic Pd and Ir, the lattice mismatch is relatively small (1.3%), which was responsible for the formation of a single-crystal structure.

The elemental distributions of Pd and Ir in octapods and nanocages were determined by EDX mapping and spectral analysis. As shown in Fig. 2e, the EDX mapping of an octapod clearly revealed a core–shell structure, with the Pd core in the center and Ir arms in the outer shell. In contrast, for the nanocage (Fig. 2f), both Pd and Ir were homogeneously distributed throughout the particle, indicating the formation of an alloy. The formation of hollow structure might be due to the dissolution of Pd from the interior, followed by re-deposition on the outer layer. The molar ratios of Ir to Pd were also derived from the EDX spectra, with the values being 0.25 and 0.50 for the octapods and nanocages, respectively. The composition analyses were also confirmed by XPS measurements. As shown in Fig. S2 (ESI†), the peaks located at 340.58 eV, 335.18 eV, 64.18 eV,

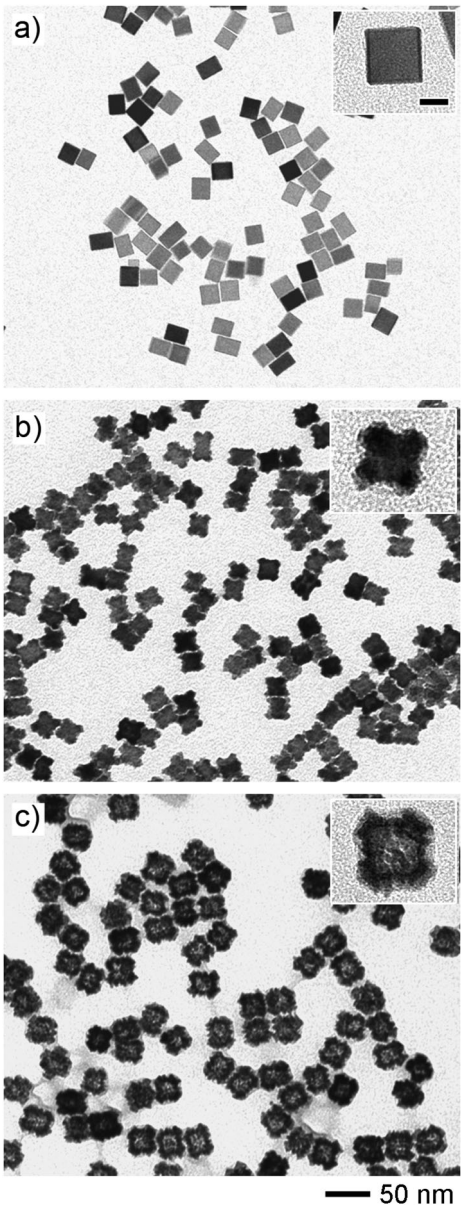

Fig. 1 TEM images of (a) Pd nanocubes with an edge length of 18 nm and (b, c) Pd–Ir bimetallic nanostructures in the forms of (b) octapods and (c) nanocages. The products were obtained at different stages of a standard synthesis stopped at (b) 2 h and (c) 24 h, respectively. The scale bar in the inset of (a) is 10 nm and applies to all other insets.

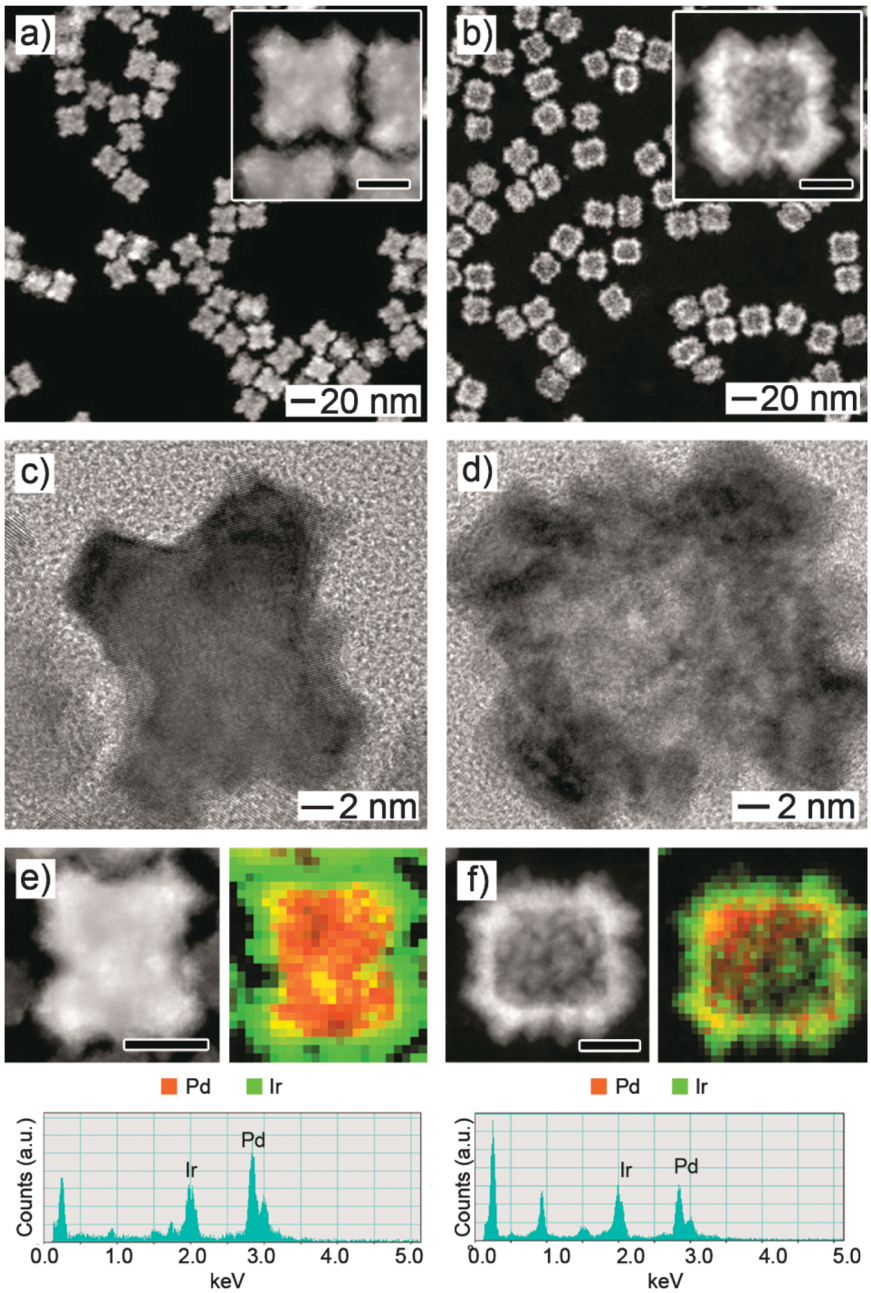

Fig. 2 Characterizations of the morphology, structure, and composition of (a, c, e) Pd–Ir core–shell octapods and (b, d, f) Pd–Ir alloyed nanocages prepared using the standard synthesis procedure: (a, b) HADDF-SEM images, (c, d) HRTEM images, and (e, f) STEM images and EDX mapping analysis. The brown and green colors in (e) and (f) correspond to elemental Pd and Ir, respectively. The scale bars are 10 nm in the insets of (a), (b), (e), and (f).

and 62.78 eV could be assigned to Pd ($3d_{3/2}$), Pd ($3d_{5/2}$), Ir ($4f_{5/2}$), and Ir ($4f_{7/2}$), respectively. Two shoulder peaks located at 342.28 eV and 336.78 eV were observed for the product sampled at t = 1 h. They could be attributed to the presence of $PdBr_4^{2-}$ on the surface of Pd nanocubes. Originally, the surface of Pd nanocubes was capped by Br^- ions.[37] As the reaction proceeded, the Pd nanocube was coated by a layer of Ir, leading to the disappearance of these two shoulder peaks at a later stage. Also, as the content of Ir increased in the product, the intensities of Ir peaks significantly increased relative to those of the Pd peaks.

For a standard synthesis, the Ir precursor solution was slowly pumped into the reaction mixture. We conducted control experiments to evaluate the impact brought by the injection rate on the morphology of the final product. As shown in Fig. 3a and b, if the Ir precursor was added in one shot by using a pipette, the final product was mixed with many tiny Ir particles. In this case, the concentration of Ir atoms could easily reach the level of supersaturation. Instead of deposition on the existing Pd cubes, it was possible for these atoms to go through homogenous nucleation and generate tiny particles in the solution. In contrast, when the pumping rate of the Ir precursor

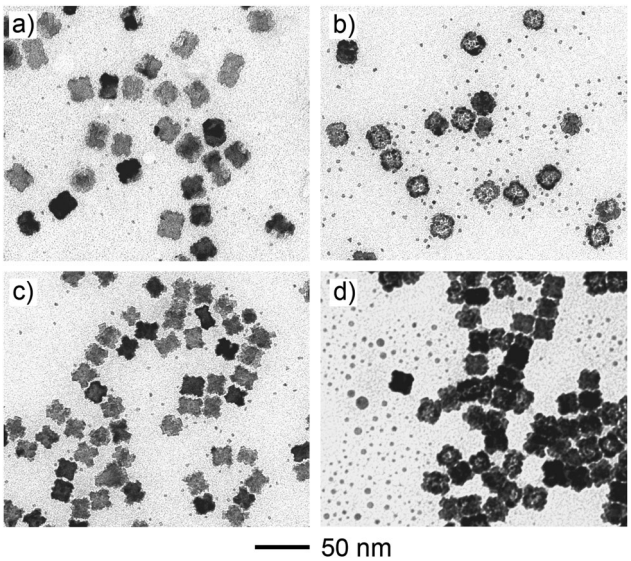

Fig. 3 TEM images of Pd–Ir bimetallic nanostructures obtained using the standard procedure except that the Ir precursor was introduced in different ways: (a, b) quick injection using a pipette and (c, d) injection at a rate of 0.75 mL h^{-1} using a syringe pump. The samples were obtained at different stages of the synthesis: (a, c) 2 h and (b, d) 24 h, respectively.

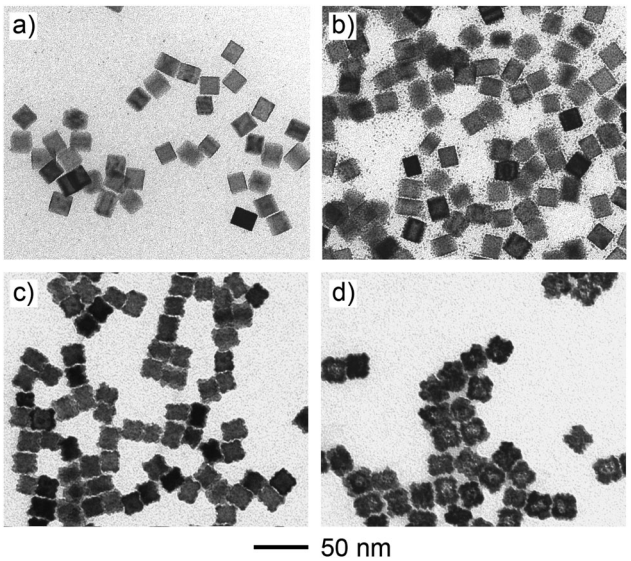

Fig. 4 TEM images of Pd–Ir bimetallic nanostructures obtained using the standard procedure except for the use of KBr in different amounts: (a, b) 0 and (c, d) 600 mg, respectively. The samples were obtained at different stages of the synthesis: (a, c) 2 h and (b, d) 24 h, respectively.

was reduced to 0.75 mL h^{-1}, large particles with broad size distribution were observed in addition to the main product (Fig. 3c and d). During the galvanic replacement, Pd atoms were oxidized and dissolved from the nanocubes in the form of Pd^{2+} cations. They could then be reduced by EG to form Pd nuclei and nanoparticles. However, the presence of Ir^{3+} ions could etch these Pd nuclei and nanoparticles back to the ionic form. At an insufficient supply of Ir^{3+} ions, the Pd nuclei could survive and thus grow into large particles with a random size distribution. Taken together, it is important to control the injection rate of the Ir precursor and thus maintain the concentrations of Ir^{3+} ions and Ir atoms within a reasonable range to avoid homogeneous nucleation of the Ir nanoparticles and enable sufficient etching towards the newly formed Pd nuclei.

We also investigate the effect of Br^- ions in our system. For instance, when KBr was absent, no obvious shape change was observed for the Pd nanocubes (Fig. 4a and b). The corners of Pd cubes were still very sharp, indicating that galvanic replacement between Ir^{3+} ions and Pd nanocubes likely did not occur. When a much larger amount of KBr was introduced (*e.g.*, 600 mg, Fig. 4c and d), no difference in shape evolution was found in comparison with the results obtained from the standard synthesis. This phenomenon was consistent with our previous study, in which Br^- was demonstrated to play an essential role in the galvanic replacement between Pd nanocubes with other types of metal ions.[35] The reaction mechanism could be summarized as follows:

$$3Pd + 2IrBr_6^{3-} = 3PdBr_4^{2-} + 2Ir$$

The reduction potential of $PdBr_4^{2-}$/Pd (0.49 eV *versus* RHE) is much lower than $IrBr_6^{3-}$ (0.86 eV *versus* RHE).[38] Therefore, it would be much easier for Pd to be oxidized in the presence of Br^-. In addition, the selective absorption of Br^- on the {100} facets of Pd nanocubes essentially induced and controlled the anisotropic deposition of Ir atoms on the {111} facets to generate the octapods.

Another important parameter for this reaction was the temperature. At a low temperature such as 100 °C, it was found that the Pd nanocubes were firstly truncated at the corners and then transformed into nanospheres with much smaller sizes (Fig. S3a and b, ESI†). In this case, the reaction rates for both galvanic replacement and co-reduction were reduced. Therefore, it became more difficult for both reactions to occur. Instead, the etching caused by Ir^{3+} in the solution played a dominant role and resulted in significant truncation at corners for the Pd nanocubes. It should be noted that Ir^{3+} was a key component for the etching process since the Pd nanocubes could still maintain their shape in the absence of an Ir precursor (Fig. S4a and b, ESI†). When the temperature was increased to 160 °C, no remarkable difference was observed in comparison with the results shown in Fig. 1b and c, except for a slight increase in roughness on the surface (Fig. S3c and d, ESI†). Taken together, an elevated reaction temperature would favor both the galvanic replacement and co-reduction, which are crucial for the sequential formation of Pd–Ir octapods and nanocages.

The size of the resultant Pd–Ir octapods and nanocages could be readily controlled by using Pd nanocubes with different sizes as the sacrificial templates. Fig. 5 shows the Pd nanocubes with average edge lengths of 10 nm and 6 nm, respectively, and their evolution into Pd–Ir octapods and nanocages by following a standard procedure. Similarly, a slight increase in size relative to the Pd nanocubes was also observed for the octapods and nanocages due to the overgrowth of Ir along the corner sites of the cubic templates.

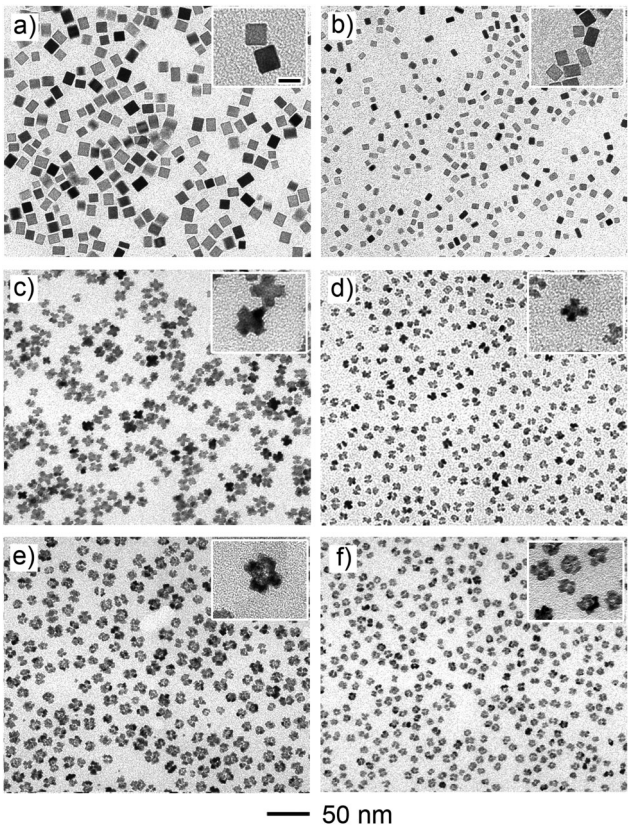

Fig. 5 TEM images of (a, b) Pd nanocubes with an edge length of 10 nm and 6 nm, respectively, and (c–f) the corresponding Pd–Ir bimetallic nanostructures in the form of (c, d) octapods and (e, f) nanocages. The reaction parameters were kept the same as for the standard synthesis except for the use of Pd nanocubes with different edge lengths. The scale bar in the inset of (a) is 10 nm and applies to all other insets.

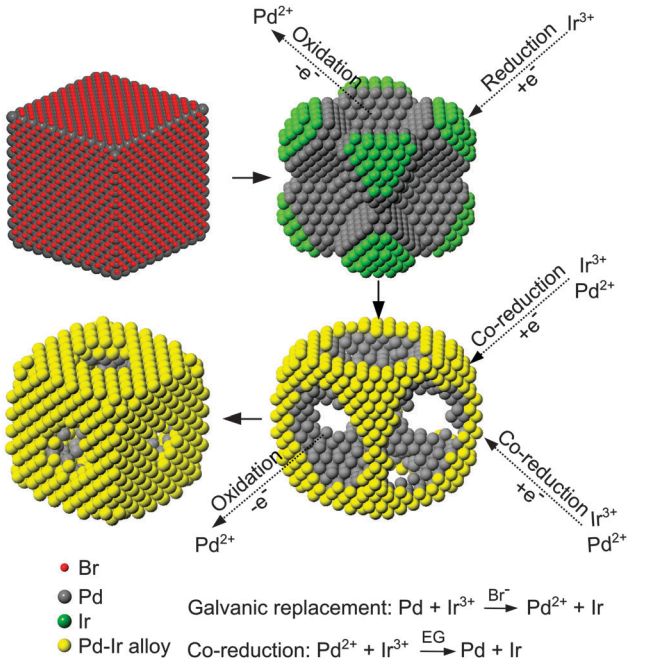

Fig. 6 Schematic illustration showing how the morphology and composition of the Pd–Ir bimetallic octapods and nanocages changed as a function of reaction time. Note that the Pd atoms in the newly formed Pd–Ir bimetallic walls were less reactive relative to the Pd atoms in the original nanocubes made of pure Pd, and thus they could survive the galvanic replacement reaction with the Ir precursor.

Fig. 6 shows a plausible mechanism responsible for the sequential formation of Pd–Ir octapods and nanocages. Briefly, the Br^--capped Pd nanocube was selectively etched from the {100} facets, accompanied by the deposition of Ir atoms on the {111} facets (corners), forming an octapod. During this period, the galvanic replacement played a dominant role while the co-reduction was suppressed due to a limited concentration of both Pd^{2+} and Ir^{3+} cations. As the concentrations of Pd^{2+} and Ir^{3+} increased in the reaction mixture, the co-reduction process became accelerated. Pd and Ir atoms were deposited onto side faces of the template to form an alloyed shell. It is worth pointing out that the newly formed Pd atoms could not be oxidized and dissolved again due to the formation of a Pd–Ir alloy. Eventually, after all the Pd in the interior have been dissolved, an alloyed nanocage with a hollow interior and porous walls was produced. A proper injection rate of Ir precursor solution, the presence of sufficient KBr, as well as an elevated temperature are all crucial for the formation of the desired products, as these parameters determined the interplay of galvanic replacement and co-reduction.

The Pd–Ir bimetallic alloyed nanocages (25 nm in size) and core–shell octapods (20 nm in size) were then tested as catalysts for selective hydrogen generation *via* the decomposition of hydrous hydrazine. The Pd nanocubes (18 nm in size) were also tested as a catalyst but no gas was produced. As shown in Fig. 7, both nanocages and octapods exhibited H_2 selectivity for this catalytic reaction. Previous studies have indicated that neither pure Pd nor Ir nanoparticles exhibited catalytic activity toward this reaction at room temperature.[22] Therefore, the hydrogen formation should be attributed to the bimetallic structures associated with both products. To our knowledge, this is the first report that Pd–Ir bimetallic nanoparticles with well-defined structure and morphology were demonstrated with selectivity for the generation of hydrogen from the decomposition of hydrazine at room temperature. Moreover, the catalytic activity of Pd–Ir nanocages was much higher than that of octapods. In particular, the molar ratios between the generated gas and the hydrazine introduced into the reaction were 2.1 and 1.1 for the nanocages and octapods, respectively, which corresponded to a H_2 selectivity of 66% and 29%. Such a significant difference can be attributed to the different surface compositions for the nanocages and octapods. As shown by EDX mapping results (Fig. 2e and f), the surface region of the Pd–Ir octapod was dominated by pure Ir while for the nanocage, both Pd and Ir could be found in the surface region. As discussed in many studies, the formation of heterometallic bonds between two metals can change the surface electronic structure of a nanocrystal, leading to great improvement in the catalytic performance.[11,22,24] Accordingly, the alloyed nanocages with the formation of a larger number of heterometallic bonds are supposed to show higher H_2 selectivity in comparison with the core–shell octapods. In addition, the highly porous

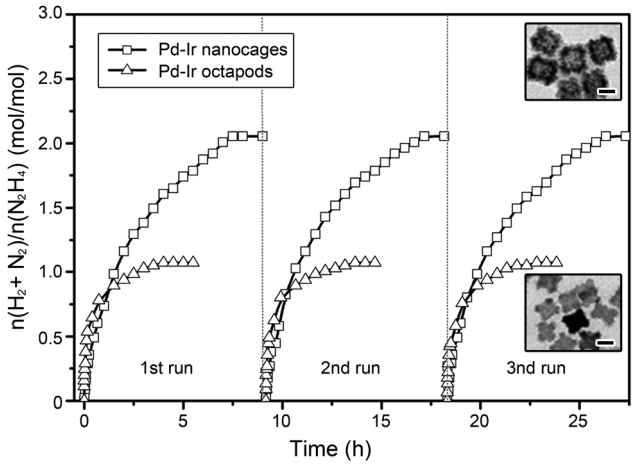

Fig. 7 Catalytic decomposition of hydrazine monohydrate to generate H_2 in the presence of 25 nm alloyed nanocages and 20 nm core–shell Pd–Ir octapods as the catalysts, respectively. The *Y*-axis refers to the mole fraction of the gas products relative to the initially added hydrazine. An additional aliquot of hydrazine hydrate was introduced into the reaction vessel after the completion of each run. The insets show TEM images of the Pd–Ir nanocages (top) and octapods (bottom) obtained after the last run of the catalytic reaction. Both scale bars are 20 nm. The morphology of these nanostructures was essentially maintained during the three rounds of reactions.

surface of a nanocage could also be of great significance for the catalytic performance since the porosity would substantially increase the specific surface area and allow for a faster transport for the reagents and products.[39,40]

We have also evaluated the catalytic performance of 14 nm Pd–Ir nanocages shown in Fig. 5e. Compared to the 25 nm Pd–Ir nanocages, the 14 nm nanocages exhibited a faster decomposition rate (Fig. S6, ESI†). Such enhanced catalytic performance could be attributed to the increased surface area for the smaller Pd–Ir alloyed nanocages. However, these smaller nanocages showed H_2 selectivity (*ca.* 67%) similar to that of the larger nanocages. This result indicated the essential role of the alloyed structure on the surface in determining the reaction selectivity.

Based on the previous reports, the mechanism involved in the decomposition of hydrazine can be summarized in Fig. S7 (ESI†).[16] Briefly, N_2H_4 molecules firstly adsorbed onto the surface of the Pd–Ir bimetallic surface, and decomposed into NH_2. The NH_2 further splits into N and H atoms, which then combined into N_2 and H_2 molecules. The newly formed N_2 and H_2 molecules finally desorbed from the crystal surface and evolved as gas products.

Conclusions

In summary, Pd–Ir bimetallic nanostructures in the forms of octapods and nanocages have been successfully prepared. The morphology, structure, and composition of both products were characterized using HAADF-STEM, HRTEM, and EDX. We systematically investigated, and at the same time, optimized the parameters involved in the reaction. In particular, a proper injection rate, a proper amount of KBr, and a relatively high temperature were found to be essential for the formation of octapods and nanocages at different stages of synthesis. The interplay of galvanic replacement between an Ir precursor and Pd nanocubes, and the co-reduction of Ir^{3+} and Pd^{2+} is considered to be essential for the formation of these two unique structures in sequence. The size of these two nanostructures could be easily controlled by using Pd cubes with different sizes. We chose the decomposition of hydrazine as a model reaction to test their catalytic performances. Specifically, with an alloyed, highly porous surface, the nanocages exhibited higher selectivity for hydrogen generation than the octapods. The combination of galvanic replacement and co-reduction provides a simple and effective means for rationally controlling the morphology of bimetallic nanostructures with a variety of different compositions.

Acknowledgements

This work was supported in part by a DOE subcontract from the University of Wisconsin at Madison (DE-FG02-05 ER15731), a grant from NSF (DMR-1215034), and startup funds from Georgia Institute of Technology. As visiting PhD students in the Xia group, M.L. (from Xi'an Jiaotong University), S.X. (from Xiamen University), and N.L. (from Southeast University) were also partially supported by the China Scholarship Council (CSC). Part of the research was conducted at the Robert P. Apkarian Integrated Electron Microscopy Core of Emory University.

References

1 A. Zuttel, A. Borgschulte and L. Schlapbach, *Hydrogen as a Future Energy Carrier*, Wiley-VCH, Weinheim, 2008.
2 Z. Xiong, C. K. Yong, G. Wu, P. Chen, W. Shaw, A. Karkamkar, T. Autrey, M. O. Jones, S. R. Johnson, P. P. Edwards and W. I. F. David, *Nat. Mater.*, 2007, **7**, 138.
3 L. Schlapbach and A. Zuttel, *Nature*, 2001, **414**, 353.
4 J. K. Dawson, *Nature*, 1974, **249**, 724.
5 M. I. Hoffert, K. Caldeira, G. Benford, D. R. Criswell, C. Green, H. Herzog, A. K. Jain, H. S. Kheshgi, K. S. Lackner, J. S. Lewis, H. D. Lightfoot, W. Manheimer, J. C. Mankins, M. E. Mauel, L. J. Perkins, M. E. Schlesinger, T. Volk and T. M. L. Wigley, *Science*, 2002, **298**, 981.
6 X. Chen, C. Li, M. Graetzel, R. Kosteckid and S. S. Mao, *Chem. Soc. Rev.*, 2012, **41**, 7909.
7 M. P. Suh, H. J. Park, T. K. Prasad and D. Lim, *Chem. Rev.*, 2012, **112**, 782.
8 M. Liu, L. Wang, G. Lu, X. Yao and L. Guo, *Energy Environ. Sci.*, 2011, **4**, 1372.
9 D. Zhong, K. Aranishi, A. K. Singh, U. B. Demirci and Q. Xu, *Chem. Commun.*, 2012, **48**, 11945.
10 E. W. Schmidt, *Hydrazine and its Derivatives: Preparation, Properties, Applications*, Wiley, New York, 2nd edn, 2001.
11 H.-L. Jiang, S. K. Singh, J.-M. Yan, X.-B. Zhang and Q. Xu, *ChemSusChem*, 2010, **3**, 541.
12 L. He, Y. Huang, A. Wang, X. Wang, X. Chen, J. J. Delgado and T. Zhang, *Angew. Chem., Int. Ed.*, 2012, **51**, 6191.

13 J. Wang, X. Zhang, Z. Wang, L. Wang and Y. Zhang, *Energy Environ. Sci.*, 2012, **5**, 6885.
14 D. G. Tong, W. Chu, P. Wu, G. F. Gu and L. Zhang, *J. Mater. Chem. A*, 2013, **1**, 358.
15 L. He, Y. Huang, A. Wang, Y. Liu, X. Liu, X. Chen, J. J. Delgado, X. Wang and T. Zhang, *J. Catal.*, 2013, **298**, 1.
16 J. P. Contour and G. Pannetier, *J. Catal.*, 1972, **24**, 434.
17 C. A. Stowell and B. A. Korgel, *Nano Lett.*, 2005, **5**, 1203.
18 B. J. Wood and H. Wise, *J. Catal.*, 1975, **39**, 471.
19 R. Costi, A. E. Saunders and U. Banin, *Angew. Chem., Int. Ed.*, 2010, **49**, 4878.
20 F. Tao, M. E. Grass, Y. Zhang, D. R. Butcher, J. R. Renzas, Z. Liu, J. Y. Chung, B. S. Mun, M. Salmeron and G. A. Somorjai, *Science*, 2008, **322**, 932.
21 S. K. Singh and Q. Xu, *J. Am. Chem. Soc.*, 2009, **131**, 18032.
22 S. K. Singh, X.-B. Zhang and Q. Xu, *J. Am. Chem. Soc.*, 2009, **131**, 9894.
23 S. K. Singh and Q. Xu, *Chem. Commun.*, 2010, **46**, 6545.
24 S. K. Singh and Q. Xu, *Inorg. Chem.*, 2010, **49**, 6148.
25 R. Narayanan and M. A. El-Sayed, *Nano Lett.*, 2004, **4**, 1343.
26 F. J. Vidal-Iglesias, J. Solla-Gullón, P. Rodrıguez, E. Herrero, V. Montiel, J. M. Feliu and A. Aldaz, *Electrochem. Commun.*, 2004, **6**, 1080.
27 M. Jin, H. Zhang, Z. Xie and Y. Xia, *Energy Environ. Sci.*, 2012, **5**, 6352.
28 Y. Zheng, J. Tao, H. Liu, J. Zeng, T. Yu, Y. Ma, C. Moran, L. Wu, Y. Zhu, J. Liu and Y. Xia, *Small*, 2011, **7**, 2307.
29 N. Tian, Z.-Y. Zhou, N.-F. Yu, L.-Y. Wang and S.-G. Sun, *J. Am. Chem. Soc.*, 2010, **132**, 7580.
30 X. Huang, Y. Li, Y. Li, H. Zhou, X. Duan and Y. Huang, *Nano Lett.*, 2012, **12**, 4265.
31 N. Tian, Z.-Y. Zhou, S.-G. Sun, Y. Ding and Z. L. Wang, *Science*, 2007, **316**, 732.
32 H. Zhang, M. Jin and Y. Xia, *Angew. Chem., Int. Ed.*, 2012, **51**, 7656.
33 M. Jin, H. Liu, H. Zhang, Z. Xie, J. Liu and Y. Xia, *Nano Res.*, 2011, **4**, 83.
34 X. Xia, S. Xie, M. Liu, H.-C. Peng, N. Lu, J. Wang, M. Kim and Y. Xia, *Proc. Natl. Acad. Sci. U. S. A.*, 2013, **110**, 6669.
35 H. Zhang, M. Jin, J. Wang, W. Li, P. H. C. Camargo, M. J. Kim, D. Yang, Z. Xie and Y. Xia, *J. Am. Chem. Soc.*, 2011, **133**, 6078.
36 H. Zhang, M. Jin, H. Liu, J. Wang, M. J. Kim, D. Yang, Z. Xie, J. Liu and Y. Xia, *ACS Nano*, 2011, **5**, 8212.
37 A. Carrasquillo Jr, J.-J. Jeng, R. J. Barriga, W. F. Temesghen and M. P. Soriaga, *Inorg. Chim. Acta*, 1997, **255**, 249.
38 J. A. Dean, in *Lange's Chemistry Handbook*, McGraw-Hill Professional, New York, 15th edn, 1998.
39 Z. Chen, M. Waje, W. Li and Y. Yan, *Angew. Chem., Int. Ed.*, 2007, **46**, 4060.
40 M. A. Mahmoud, F. Saira and M. A. El-Sayed, *Nano Lett.*, 2010, **10**, 3764.

Supporting Information for

Facile synthesis of Pd-Ir bimetallic octapods and nanocages through galvanic replacement and co-reduction, and their use for hydrazine decomposition‡

Maochang Liu,[ab] Yiqun Zheng,[c] Shuifen Xie,[a] Naixu Li,[a] Ning Lu,[d] Jinguo Wang,[d] Moon J. Kim,[d] Liejin Guo,[b] and Younan Xia*[ac]

[a]*The Wallace H. Coulter Department of Biomedical Engineering, Georgia Institute of Technology and Emory University, Atlanta, Georgia 30332, United States.*

[b]*International Research Center for Renewable Energy, State Key Laboratory of Multiphase Flow, Xi'an Jiaotong University, Xi'an, Shaanxi 710049, P. R. China*

[c]*School of Chemistry and Biochemistry, School of Chemical and Biomolecular Engineering, Georgia Institute of Technology, Atlanta, Georgia 30332, United States*

[d]*Department of Materials Science, University of Texas at Dallas, Richardson, Texas 75080, United States*

**Corresponding author. E-mail: younan.xia@bme.gatech.edu*

The H_2 selectivity of a catalyst

Generally, hydrazine can be decomposed to generate a mixture of N_2 and H_2 (Eq. 1) or a mixture of NH_3 and N_2 (Eq. 2). The overall reaction is expressed as Eq. (3). Since the reaction according to Eq. (2) does not generate H_2, the H_2 selectivity, x, of a catalyst can be defined as the percentage of decomposition according to Eq. (1). When NH_3 is removed from the gas mixture, the H_2 selectivity can be calcualted from the amounts of N_2 and H_2 based on Eqs. (4) and (5).

$$N_2H_4 = N_2 + 2H_2 \quad (1)$$

$$3N_2H_4 = 4NH_3 + N_2 \quad (2)$$

$$3N_2H_4 = 4(1-x)NH_3 + (1+2x)N_2 + 6xH_2 \quad (3)$$

$$n(N_2+H_2)/n(N_2H_4)=[(1+2x) + 6x]/3 \quad (4)$$

$$x = [3n(N_2+H_2)/n(N_2H_4)-1]/8 \times 100\% \quad (5)$$

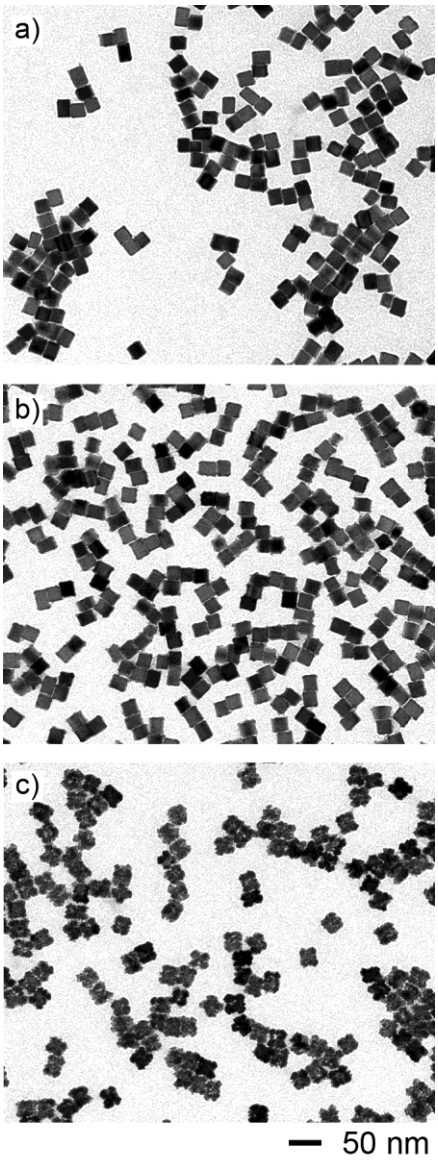

Fig. S1 TEM images of Pd-Ir bimetallic nanostructures obtained at different stages of a standard synthesis: a) 0.5 h, b) 1 h, and c) 9 h. The scale bar applies to all images.

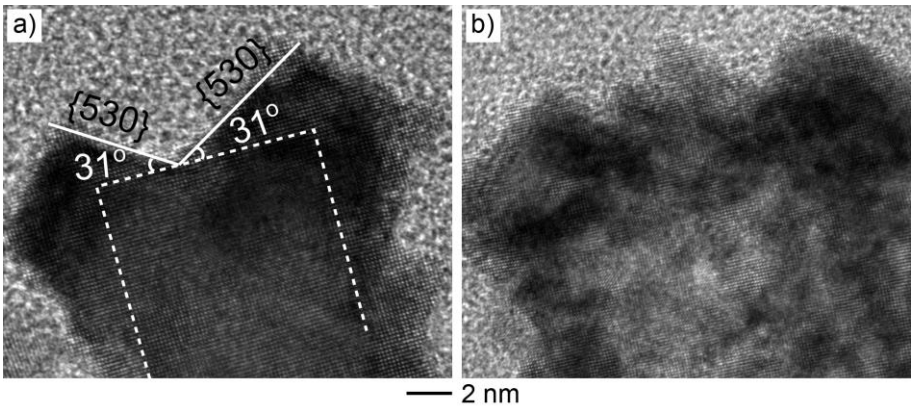

Fig. S2 High-resolution TEM images of the octapod and cage shown in Fig.2, c and d.

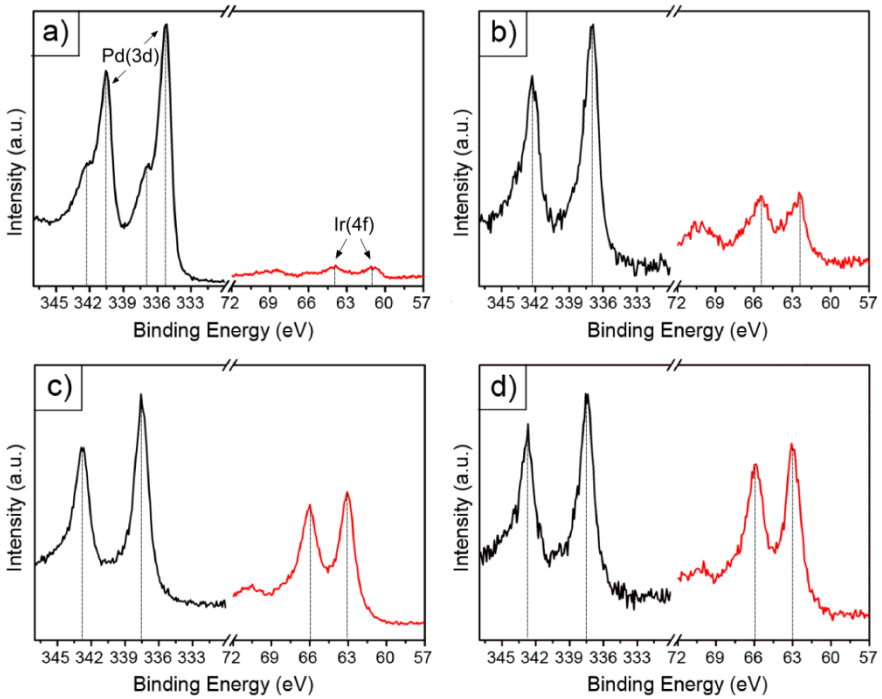

Fig. S3 X-ray photoelectron spectra (XPS) of Pd-Ir bimetallic nanostructures obtained at different stages of a standard synthesis: a) 1 h, b) 2 h, c) 9 h, and d) 24 h. Black and red curves correspond to elemental Pd and Ir, respectively.

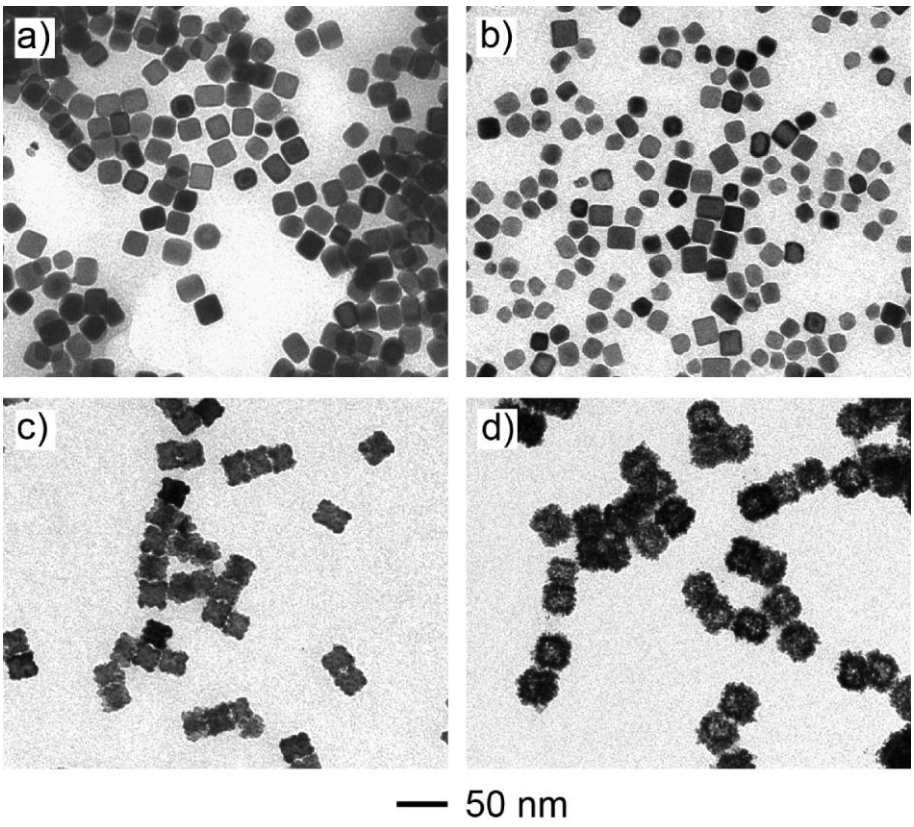

Fig. S4 TEM images of Pd-Ir bimetallic nanostructures obtained using the standard procedure, except that the reaction temperature was set to a, b) 100 ^{o}C and c, d) 160 ^{o}C, respectively. The products were obtained at different stages of the syntheses: a, c) 2 h and b, d) 24 h.

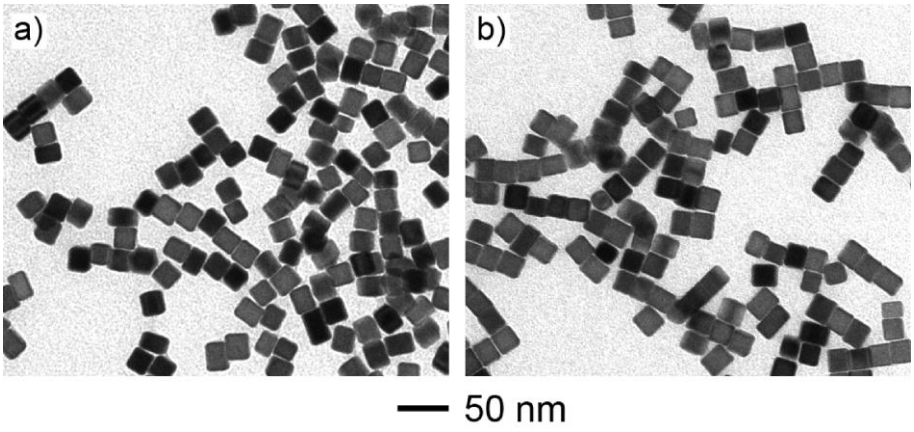

Fig. S5 TEM images of Pd nanostructures obtained from a standard synthesis, in which no Ir precursor was added. The samples were obtained at different stages of the same synthesis: a) 2 h and b) 24 h, respectively.

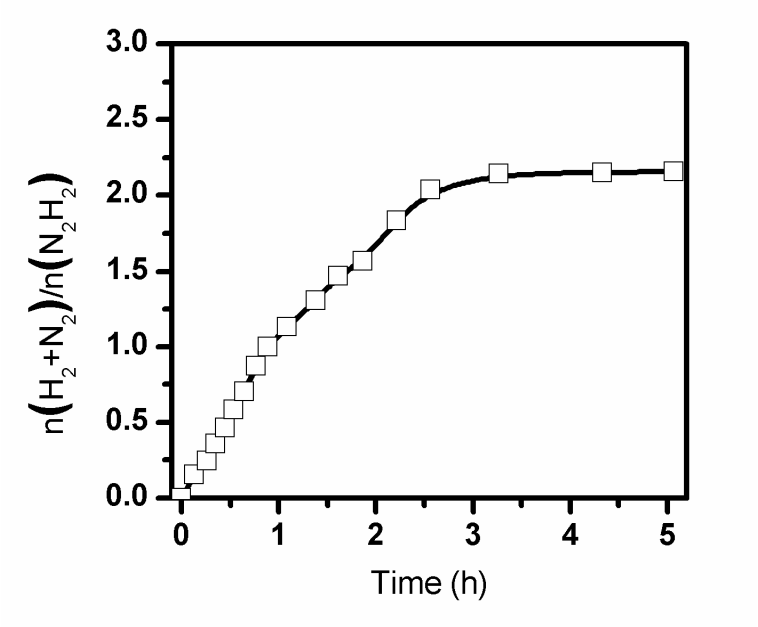

Fig. S6 Catalytic decomposition of hydrazine monohydrate to generate H_2 in the presence of 14-nm Pd-Ir nanocages as a catalyst.

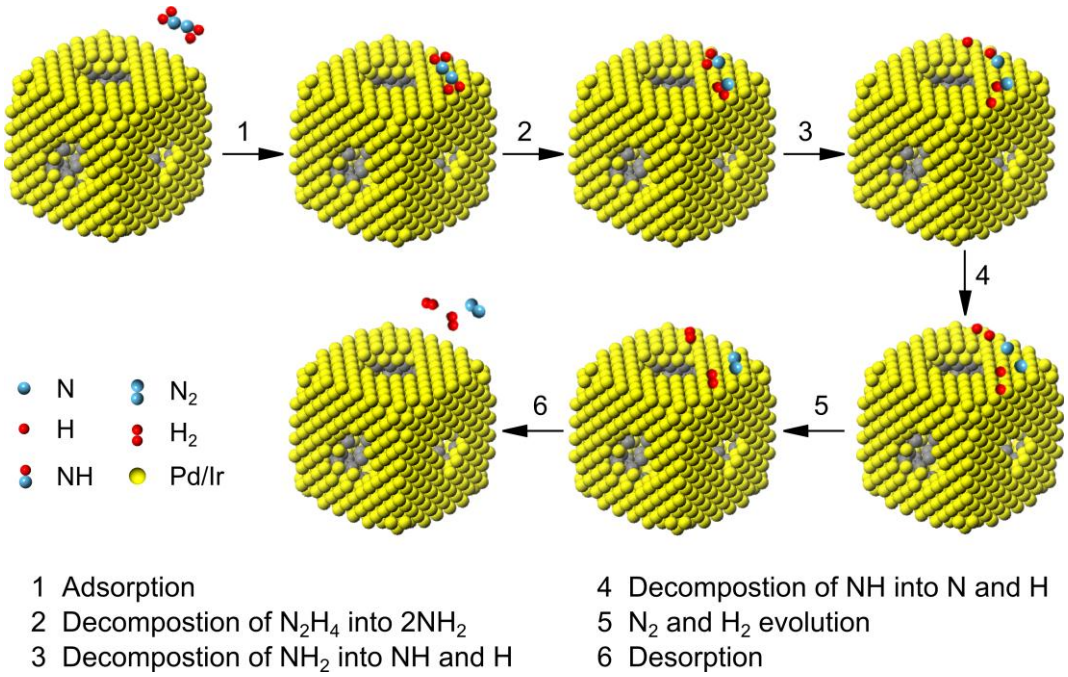

Fig. S7 A plausible mechanism involved in the decomposition of N_2H_4 over a Pd-Ir alloyed nanocage.